https://doi.org/10.20965/ijat.2019.p0679

Paper:

Improved Method for Synchronizing Motion Accuracy of Linear and Rotary Axes Under Constant Feed Speed Vector at End Milling Point – Investigation of Motion Error Under NC-Commanded Motion –

Takamaru Suzuki*,†, Kazuki Yoshikawa*, Toshiki Hirogaki*, Eiichi Aoyama*, and Takakazu Ikegami**

*Department of Mechanical Engineering, Doshisha University
1-3 Tataramiyakodani, Kyotanabe-shi, Kyoto 610-0394, Japan
†Corresponding author, E-mail: takamaru0427suzuki@yahoo.co.jp
**DMG MORI Co., Ltd., Yamatokoriyama, Japan
[Received July 17, 2018; accepted June 20, 2019]

A 5-axis machining center (5MC) is noted for its synchronous control capability, making it a feasible tool for quickly and accurately machining complicated three-dimensional surfaces such as propellers and hypoid gears as it is equipped with a direct-drive (DD) motor in the rotary axis. The current research work identified the necessity of improving both the accuracy of the machined shape and the consistency of the free-form machined surface. A method for maintaining the feed speed vector at the milling point by controlling two linear axes and the rotary axis of a 5MC to improve the quality of the machined surface was investigated. Additionally, a method was proposed for reducing the shape error of machined workpieces by considering differences in the servo characteristics of the three axes. The shape error was significantly reduced by applying the proposed method using a precedent control coefficient determined via calculations. To maintain the feed speed vector at the milling point in the machining of complex shapes, rapid velocity change in each axis is often required, leading to inaccuracy caused by torque saturation at a DD motor in the rotary axis. The results of this study indicate that torque saturation can be evaluated via simulation and that the machining accuracy and consistency can be improved by accounting for these errors using the proposed precedent control coefficient method.

Keywords: 5-axis machining center, synchronous motion, machined shape error, servo, torque saturation

1. Introduction

Recently, the 5-axis machining center (5MC), which is equipped with three linear axes and two rotary axes of motion, has become a widely accepted manufacturing technology [1, 2]. Currently, the rotary axes are typically used as indices, and work is most often performed using only the three linear axes. However, 5MCs are notable for their synchronous control capability, which makes them feasible for rapidly machining complex three-dimensional surfaces such as propellers and hypoid gears [3, 4]. In recent years, research has been conducted to reduce the declination from the ordered trace and to improve the geometric accuracy of machining motion by using advanced and high-precision contouring controls, as well as by adjusting parameters [5–7]. However, there has been little research into processing technology that provides synchronous control using both linear and rotary axes. As indicated by previous studies, it is necessary to improve not only the machined shape accuracy but also the machined surface roughness of free-form surfaces. In particular, it is important to maintain a consistent surface roughness over an entire machined surface. A method for maintaining the surface quality of a machined curved surface has been proposed that utilizes the synchronous motion characteristics of a 5MC to coordinate motion between two linear axes and a rotary axis, as this level of quality is difficult to accomplish with a three-axis machining center (3MC) [8, 9]. This method can effectively control the surface roughness of the entire machined surface because a computer numerical control (CNC) program is used to maintain the feed speed vector at the milling point on the surface at a constant speed and direction. This method can prevent errors parallel to the feed speed vector at the milling point, such as a quadrant projection, from affecting the shape error. Additionally, because the relative position between the workpiece and tool remains unchanged and the cutting point receives a fixed quantity of air, this method can retain the involution of the chip. Moreover, although 5MCs generally have static rigidity, heat transformation, motion rigidity, orthogonality, and anisotropy, this method can reduce their influence by keeping the magnitude and direction of the cutting resistance constant. However, the causes of errors that can influence the quality of the machined shape when CNC is employed have

not been discussed.

To address this gap in understanding, in the present study, CNC precedent control (Pre-Control) was used to cut a circular shape with the objective of investigating the causes of shape error, and then a processing method for reducing this shape error was developed. First, an equation was developed to model the shape error using a predicted cause of error. Second, the validity of this assumption was examined using data from CNC machining tests. In the final step, the most appropriate processing method was determined via a comparison of machining results. The results indicated that the observed error was caused by a decrease in the circle radius due to the circular interpolation motion between the two linear axes and a relative angle difference between the linear axes and the rotary axis. Accordingly, a method for solving the shape error of machined workpieces that considers the differences between the servo characteristics of these three axes was proposed. To reduce the influence of these factors even in the case of high-angular-velocity movement, a theoretical method was developed to determine the most suitable K_{FFP} (precedent control coefficient) of each axis by using a block diagram that considers torque saturation. Although various disturbances occur during workpiece cutting, in this study, we focused on investigating the motion error under numerical control (NC)-commanded motion as the first step to diagnose many factors. However, it is considered that the method developed in this study has a certain effect because the processing load is extremely small in the case of cutting a soft metal for finishing [10].

2. Definitions

2.1. Definition of Contour Line (CL) [9]

The CL tool path in a 3MC is defined as the line tracing an offset surface that is in contact with the tool and the intersecting plane that is perpendicular to the Z-axis. However, in 5MCs, the CL cannot be defined this way, because the relationship between the workpiece position and the Z-axis may change depending on the rotary axis control. Therefore, in this study, the CL was defined as the line given by the intersection of the offset surface in contact with the tool and the plane perpendicular to the central axis O_W of the workpiece, as shown in **Fig. 1**.

2.2. Feed Speed Vector at Cutting Point

The feed speed in the cutting of an endmill is generally the velocity of the center of the endmill tool. The feed speed F of the central axis of the tool and the feed speed F_C at the cutting point are equal in the cutting of a flat plane, as shown in **Fig. 2(a)**, but they are not equal in the cutting of a curved surface, as shown in **Fig. 2(b)**. The cutting phenomenon changes depending on the curvature of the workpiece. It was considered necessary to focus on this phenomenon, as it affects the surface quality. To this end, a new definition of the feed speed at the cutting point is proposed. **Fig. 3** depicts the feed speed vector

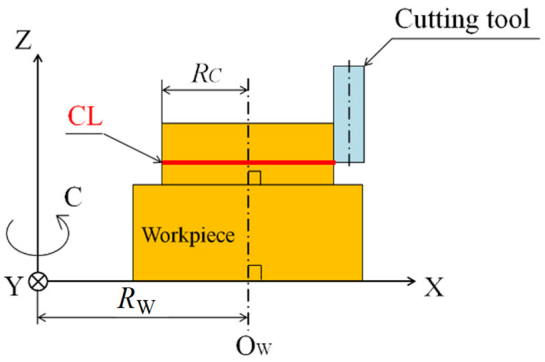

Fig. 1. Definition of the CL for a 5MC (X-Z plane).

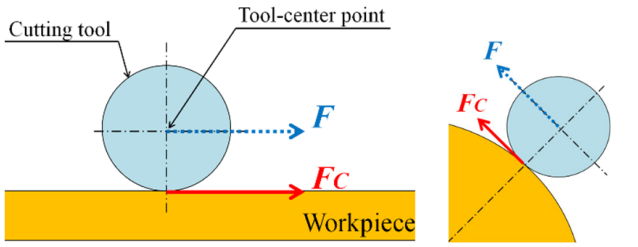

(a) Flat surface (b) Curved surface

Fig. 2. Flat- and curved-surface machining.

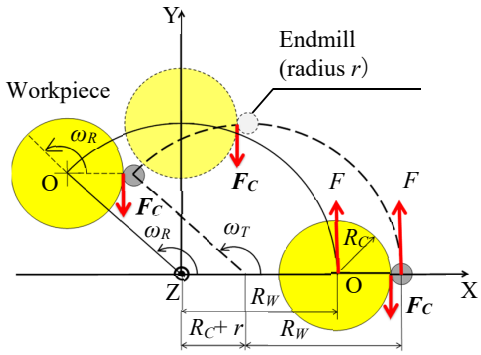

Fig. 3. Trajectory of motion under a constant feed speed vector at the cutting point (X-Y plane, P-P' section).

at the cutting point, defining a tangent vector as the feed speed F_C at the cutting point in Section P-P', which includes the cutting point at right angles to the central axis of the endmill.

However, in the case of cutting workpieces with irregular surfaces, it is impossible to maintain the feed speed at the cutting point, because the rotary axis momentarily turns the other way when its angular velocity is zero, as shown in **Fig. 4**.

2.3. Definition of Constant Feed Speed Vector at Cutting Point [11–13]

Figure 3 presents a model diagram for cutting the outline of a circle in two dimensions, where F_C represents

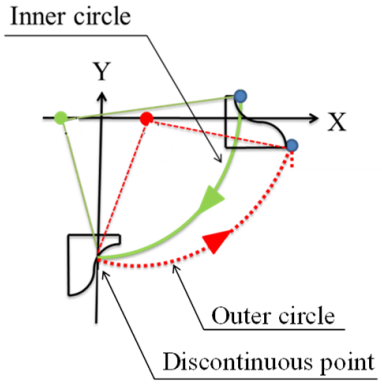

Fig. 4. Cutting a workpiece with an irregular surface.

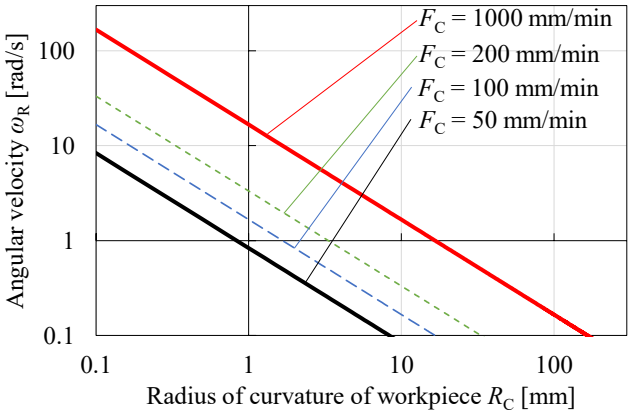

Fig. 5. Relationship between the radius of curvature and the angular velocity.

the feed speed at the cutting point, R_C represents the radius of curvature of the workpiece, and ω_R represents the angular velocity of the C-axis. Clearly, ω_R can be derived from F_C and R_C as follows:

$$\omega_R = \frac{F_C}{R_C}. \quad \ldots\ldots\ldots\ldots\ldots\ldots \quad (1)$$

If F represents the command feed speed of the center of the tool, R_W represents the distance from the origin of the machine coordinate system to the center of curvature, and ω_T represents the angular velocity of the center of the tool. ω_T can be derived from F and R_W as follows:

$$\omega_T = \frac{F}{R_W}. \quad \ldots\ldots\ldots\ldots\ldots\ldots \quad (2)$$

If ω_R and ω_T are equal, the feed speed vector at the cutting point is constant and can be expressed as:

$$\frac{F_C}{R_C} = \frac{F}{R_W}. \quad \ldots\ldots\ldots\ldots\ldots\ldots \quad (3)$$

In this study, the feed speed vector at the cutting point was considered in the case of a constant R_C, R_W, F, and ω_R.

2.4. Required Angular Velocity and Moment of Inertia of Load Around Rotary Axis of Table

In this study, the objective was to maintain the feed speed vector at the milling point in the machining of complex shapes. When machining complex shapes in this manner, it is generally difficult to realize high synchronous control, because of rapid velocity changes in each axis. Typically, methods for maintaining the feed speed vector at the milling point are employed at low feed speeds ($\leq$100 mm/min) at the cutting point [14, 15]. This approach is generally avoided because of the low productivity resulting from the required low feed speed. A method that can realize high synchronous control without reducing the feed speed to 100 mm/min would result in an increase in the industrial value of high synchronous control.

Initially, the required angular velocity of the C-axis ω_R [rad/s] was considered. **Fig. 5** depicts the relationship between R_C and ω_R derived from Eq. (1). Here, it can be observed that there is a proportional relationship between F_C and R_C and that there is an inverse relationship between F_C and ω_R. A higher F_C and smaller R_C yield a higher ω_R. Considering that the required F_C is 200 mm/min, which is higher than the feed speed often used in this method, the required ω_R is 10.0 rad/s (3.2π rad/s) (from **Fig. 5**) when the radius of curvature of the workpiece is approximately 0.5 mm. Moreover, because the acceleration/deceleration time for this transition is generally 0.1 s, the maximum value of the angular acceleration is 143 rad/s^2 for maintaining the feed speed vector at the milling point; thus, an extremely high motor torque is needed [16]. Therefore, when machining complex shapes using this method, rapid velocity changes in the rotary axis are inevitable; hence, the rotary axis can be considered the key axis for improving synchronous precision.

In applying the proposed synchronous control method, the focus was on not only the angular acceleration but also the moment of inertia of the load around the rotary axis of the table. The 5MC is often used for machining complex shapes, such as molds. It often requires high-precision machining with microscale accuracy, and the moment of inertia relative to the center of the rotary axis of the table is 5.0 kg·m^2.

Thus, for increasing the practicability of the proposed synchronous control method, a high moment of inertia of the load around the rotary axis of the table should be assumed.

3. Experimental Methods

In this study, NMV5000 (DMG MORI Co., Ltd.) 5MC CNC was used (**Fig. 6**). The machining center could move along three linear axes (X,Y,Z) and two rotary axes (B,C). The B- and C-axes were driven by direct-drive (DD) motors. Two linear axes (X,Y) and a rotary axis C were used. **Fig. 3** shows the trajectory of motion for the tests. The feed speed vector was kept constant at the cutting point. In this state, the condition

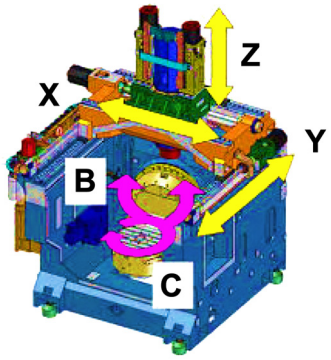

Fig. 6. Model of the 5MC used in this study.

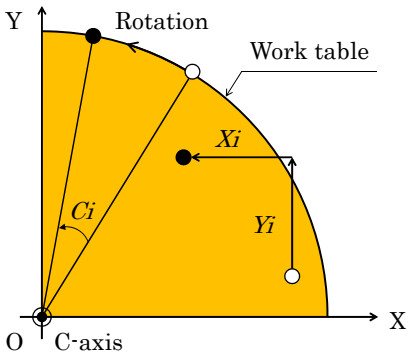

Fig. 7. Values measured by SERVO GUIDE.

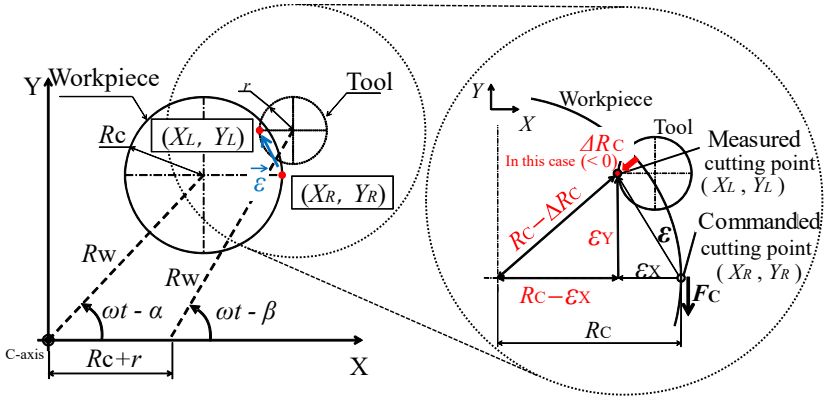

Fig. 8. Geometric model for determining the shape error.

$F_C : F = R_C : R_W$ can be satisfied. The selected feed speed vector was parallel to the Y-axis in the negative direction. The total moment of inertia $J + J_1$ was changed by applying three different work patterns with moments of inertia of $J_1 = 1.70$, 3.24, and 4.77 kg·m^2 acting around the rotary axis of the table. In these tests, the radius R_C of the circles was 5 mm, and the offset R_W was 8 mm. The angular velocity ω was changed to 0.5π, π, 1.5π, 2π, 3π, and 4π rad/s, and the feed speed F was changed to 754, 1507, 2261, 3014, 4522, and 6029 mm/min. The default value of the position proportional gain K_{pp} was 30 in all axes.

4. Analysis Methods

4.1. Evaluation Method

The CNC tuning software SERVO GUIDE was used to obtain NC data from the 5MC. This software measured displacement from the starting measurement position at given intervals during a previously defined cycle. In this experiment, the location (X_i, Y_i) (in mm) along the linear axes (X, Y) and C_i (in degrees) around the rotary axis C were measured at 1 ms intervals, as shown in **Fig. 7**.

Figure 8 depicts the relationship between the measured cutting point (X_L, Y_L) and the commanded cutting point (X_R, Y_R). The measured cutting point was the response of the position of the servomotor, and the commanded cutting point was the commanded position. The point where the straight line connecting the center of the workpiece to the center of the tool crossed the outer circumference of the tool is the measured cutting point. However, for simplification, the left edge of the tool was defined as the measured cutting point. When a gap occurred between the two points, an error vector $\boldsymbol{\varepsilon}(\varepsilon_X, \varepsilon_Y)$ was generated between them. The components of this error vector were defined as

$$\begin{cases} \varepsilon_X = X_L - X_R, \\ \varepsilon_Y = Y_L - Y_R. \end{cases} \quad \cdots\cdots\cdots\cdots \quad (4)$$

In these tests, the Pythagorean theorem was employed to evaluate the right-angled triangle generated using the center of curvature and the two cutting points as its apexes.

$$(R_C - \Delta R_C)^2 = (R_C - \varepsilon_X)^2 + \varepsilon_Y{}^2. \quad \cdots\cdots \quad (5)$$

Here, ΔR_C represents the shape error. In expanding this expression, $\Delta R_C{}^2$, $\varepsilon_X{}^2$, and $\varepsilon_Y{}^2$ can be approximated as zero when it is assumed that $\Delta R_C{}^2$, $\varepsilon_X{}^2$, and $\varepsilon_Y{}^2 \ll 1$. Then, the shape error ΔR_C is similar to the X-component of the error vector $\boldsymbol{\varepsilon}$ as

$$\Delta R_C(t) \cong \varepsilon_X(t) = X_L(t) - X_R(t). \quad \cdots\cdots \quad (6)$$

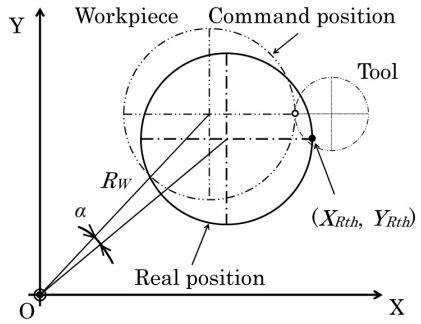

(a) Rotary axis

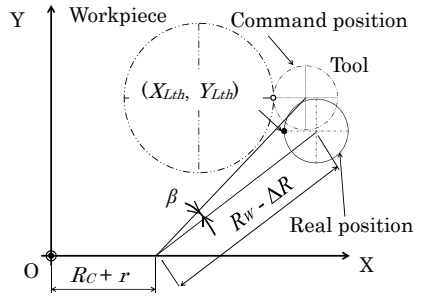

(b) Linear axes

Fig. 9. Angle-difference model for the delay of the response of each axis.

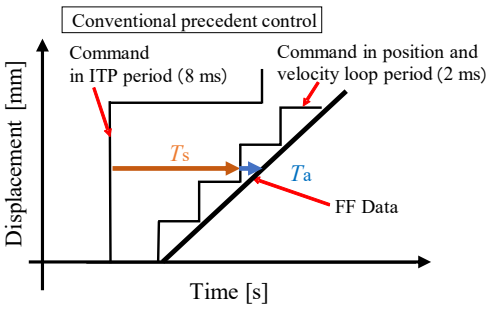

(a) Conventional precedent control

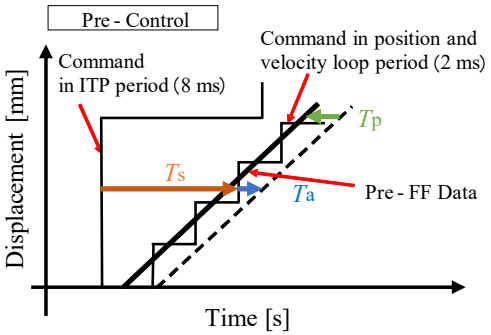

(b) Pre-Control

Fig. 10. New precedent control model.

4.2. Shape Error Expression

Initially, we focused on the frequency inputs in the linear axes and the lamp input in the rotary axis, and all error factors that could influence the shape were considered. There were three possible error factors, as follows.

- Radius decrease caused by the arc motion (frequency response) of the linear axes, ΔR [μm], >0 [17].
- Angle difference caused by reply delay of the lamp input of the rotary axis, α [mrad], >0 (**Fig. 9(a)**).
- Angle difference caused by reply delay of the trigonometric function of the linear axes, β [mrad], >0 (**Fig. 9(b)**).

When $\alpha \neq \beta$, the error is particular to the 5MC process. The coordinates of the cutting points in these error factors were derived as functions of time, and emphasis was placed on the importance of the X-coordinate of each cutting point as a result of Eq. (6). The expression $X_{Rth} = R_W \cos(\omega t - \alpha) + R_C$ was then valid with respect to the rotary axis, and $X_{Lth} = (R_W - \Delta R)\cos(\omega t - \beta) + R_C$ was valid with respect to the linear axis. Here, X_{Rth} and X_{Lth} were substituted for the variables X_R and X_L in Eq. (6). In expanding these expressions, a primary approximation of the trigonometric function was performed, and it was assumed that the product of the error quantities was close to 0, considering their small size. The theoretical shape error can then be expressed as

$$\Delta R_{Cth}(t) \approx -(\alpha - \beta)R_W \sin \omega t - \Delta R \cos \omega t, \quad . \quad (7)$$

where $t = 0$ is the time at which movement began, assuming that there was no dead time. Then, the phase delay of the rotary axis and the linear axes can be expressed as

$$\alpha = \omega t - \tan^{-1} \frac{Y_R}{X_R - R_C}, \quad . . . . . (8)$$

$$\beta = \omega t - \tan^{-1} \frac{Y_L}{X_L - R_C}. \quad . . . . . (9)$$

In these equations, the difference between α and β can be expressed as

$$\alpha - \beta = \tan^{-1} \frac{Y_L}{X_L - R_C} - \tan^{-1} \frac{Y_R}{X_R - R_C}. \quad . . (10)$$

Therefore, the radius decrease can be expressed as

$$\Delta R = \sqrt{(X_L - R_C)^2 + {Y_L}^2} - R_W. \quad . . . . . (11)$$

The phase delays of the rotary and linear axes, the difference between α and β, and the radius decrease were then calculated using Eqs. (8) and (9), Eqs. (10) and (11), respectively.

4.3. General Method for Reducing Shape Error

In Section 4.2, it was assumed that the main factors contributing to the shape error were a decrease in the radius and a relative angle difference. It is theorized that the shape error can be reduced by reducing these factors. To reduce the shape error, the precedent control of the 5MC is typically used. However, an averaging delay T_a [s] occurs when the order level is averaged to lower speed errors from the precedent control based on the conventional digital control, as shown in **Fig. 10(a)**. Here, ITP

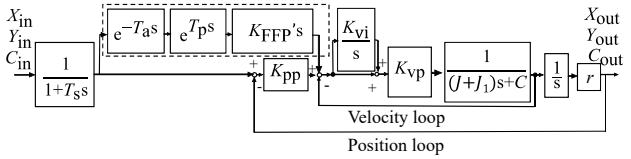

Fig. 11. Block diagram of the feed drive system.

is an interpolation period in it. However, the new precedent control (Pre-Control) improves the T_a by reading the preceding NC data for T_p, as shown in **Fig. 10(b)**. Using Pre-Control, the flatness characteristics are improved compared with the case of the conventional precedent control. Thus, the use of a Pre-Control function to reduce the shape error was considered appropriate for this study.

In a previous study [18], Pre-Control was used, and a Pre-Control coefficient (K_{FFP}) of 100% was determined as an initial set point that provided a reduced error resulting from a radius decrease and improved phase delay along each axis over the new precedent control. However, the error due to the relative angle difference was not improved at all, indicating that the shape error was not improved using Pre-Control.

Pre-Control has been successfully applied to decrease the gap between the intended machine movement and its actual movement, and it is effective for improving precision. However, the use of Pre-Control at an initial set point is poorly suited for improving the synchronization of movement along each axis.

4.4. Experimental Method for Reducing Shape Error

As discussed in Section 4.3, the shape error is not improved by using only Pre-Control at an initial set point. Therefore, it is important to develop a method to decrease the relative angle difference for effectively reducing the shape error.

To accomplish this objective, the reduction of relative angle difference $(\alpha - \beta)$ by setting K_{FFP} appropriately for each axis is proposed. The trial-and-error process of experimentally determining the most appropriate value of K_{FFP} is time-consuming; thus, a model including Pre-Control was constructed for theoretically determining the optimal values for K_{FFP}.

4.5. Modeling of Pre-Control

Figure 11 presents a block diagram of the feed drive system of the 5MC, including both the rotary and linear axes. This model is a single-degree-of-freedom system and is generally applied to the control of the linear axes [19, 20]. **Table 1** presents the values for the parameters in **Fig. 11**. These parameters were identified using simulation software. $G_R(s)$ was defined as the transmission function of the rotary axis, and $G_L(s)$ was defined as the transmission function of the linear axis. K_{pp}, K_{vp}, K_{vi}, K_{FFP}, and T_s were the set values of NC. J, C, T_a, and T_p were determined in the values to be matched with the transient state of the motion in **Fig. 3**. In the case of considering the inclination of the B-axis, the frequency inputs are needed in the X-, Y-, and Z-axes, and a clause for the load torque due to the gravity of the workpiece must be inserted behind the speed loop.

Table 1. Parameters of the model of the feed drive.

Parameter	Unit	X	Y	C
J (Equivalent inertia of mechanism)	kg·m^2	4.5	5.0	4.2
J_1 (Inertia road)	kg·m^2	–		$*$
C (Viscous damping coefficient)	Nms/rad	1.0		5.0
K_{pp} (Position proportional gain)	rad/ms or 1/s	60		60
K_{vp} (Velocity proportional gain)	Nms/rad	177.5		4700
K_{vi} (Velocity integrator gain)	Nms/rad	0.198		0.274
K_{FFP} (Prefeedforward coefficient)	%	$*$		$*$
K_{FFP}' (Prefeedforward gain)	1/s	$K_{FFP} \times K_{FF}/100$		
K_{FF} (Feedforward gain)	1/s	$2\pi/l$		1
l (Lead of ball screw)	m	0.016		–
r (Transformation coefficient)	m/rad	$l/2\pi$		1
T_s (Smoothing time constant)	s	0.05		0.064
T_a (Averaging time constant)	s	0.015		0.015
T_p (Preceding time constant)	s	0.0155		0.005

$*$set value

4.6. Derivation of Theoretical Radius Decrease and Relative Angle Difference

The theoretical radius decrease ΔR_{th} [μm] was determined by the angular velocity ω [rad/s], the gain $|G_L(j\omega)|$ in the transmission function of the linear axis $G_L(s)$, and the radius of order R_W [mm]:

$$\Delta R_{th} = (1 - |G_L(j\omega)|) \times R_W \times 10^3. \quad \ldots\ldots (12)$$

Next, to define the phase delay of the rotary axis, the steady-state error was defined, as follows. In the case of a closed-circuit system of direct connection feedback, the steady-state error is generally defined as

$$\lim_{s\to 0} sE(s) = \lim_{s\to 0}\left(\frac{s}{1+G(s)} \cdot F(s)\right). \quad \ldots\ldots (13)$$

$G_R(s)$ is a closed-loop transfer function and is converted into the closed-loop $G(s)$ as follows:

$$\frac{G(s)}{1+G(s)} = G_R(s), \quad \ldots\ldots (14)$$

$$G(s) = \frac{G_R(s)}{1-G_R(s)}. \quad \ldots\ldots (15)$$

Considering the lamp input in the rotary axis,

$$F(s) = \frac{\omega}{s^2}. \quad \ldots\ldots (16)$$

Therefore, the phase delay of the rotary axis is defined as

$$\alpha_{\text{th}} = \lim_{s\to 0}\left(\frac{s}{1+\dfrac{G_R(s)}{1-G_R(s)}}\cdot\frac{\omega}{s^2}\right) \quad \ldots\ldots (17)$$

The phase delays of the linear axes, considering the trigonometric function input in the linear axes, can then be defined as

$$\beta_{\text{th}} = -\angle G_L(j\omega) \quad \ldots\ldots (18)$$

Using Eqs. (17) and (18), considering that the relative angle difference is determined by calculating the difference between the phase delays of the rotary and linear axes, the relative angle difference can be expressed as

$$\alpha_{\text{th}} - \beta_{\text{th}} = \lim_{s\to 0}\left(\frac{s}{1+\dfrac{G_R(s)}{1-G_R(s)}}\cdot\frac{\omega}{s^2}\right) + \angle G_L(j\omega). \quad \ldots\ldots (19)$$

4.7. Best K_{FFP} Method [18]

Using the proposed models, a method for identifying the most suitable K_{FFP} at which the relative angle difference $(\alpha_{\text{th}} - \beta_{\text{th}})$ is zero was developed. This method is called the Best K_{FFP} Method. Considering that the relative angle difference is determined by calculating the difference between the phase delays of the rotary and linear axes, the algorithm of this method is:

$$(C_{\text{in}} - G_R C_{\text{in}}) - \angle G_L(j\omega) = 0, \quad \ldots\ldots (20)$$

where G_R and G_L represent transfer functions of the rotary axis and the linear axes, respectively, and C_{in} and ω represent the lamp input of the rotary axis and angular momentum functions, respectively, of time t.

5. Results and Discussion

5.1. Discussion of Cause of Shape Error

Figure 12 depicts the shape error (vertical axis) with respect to time (horizontal axis) for the following conditions: $J + J_1 = 5.9$ kg·m^2, $\omega = \pi$ rad/s, and $d\omega/dt = \pi/0.064$ rad/s^2. In the experiments, a radius decrease clearly had a significant influence on the shape error. A reduction in the radius decrease ΔR was accomplished by compensating for the command radius of the

circular interpolation control. The shape error manifested as a sine wave whose amplitude was determined by the offset R_W and the relative angle difference $(\alpha - \beta)$. However, **Fig. 12** does not show the tendency of a simple sine wave; the relative angle difference was investigated to determine the reason for this. **Fig. 13** depicts the relative angle difference (vertical axis) over time (horizontal axis). A spike-shaped shape error is observed at 129 ms in **Fig. 12**, corresponding to a spike-shaped relative angle difference in **Fig. 13**. The presence of a spike-shaped relative angle difference is an indication of a difference in the

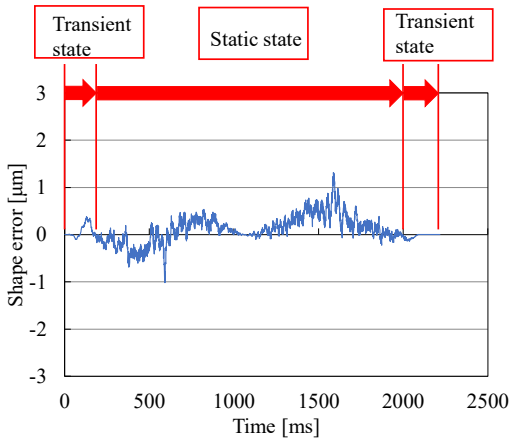

Fig. 12. Experimental results for the shape error under the following conditions: $J + J_1 = 5.9$ kg·m^2 and $\omega = \pi$ rad/s.

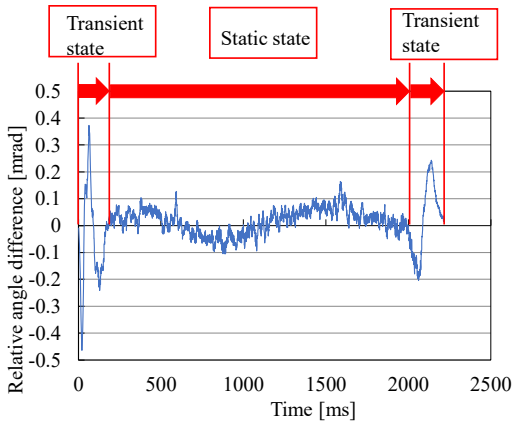

Fig. 13. Experimental results for the relative angle difference under the following conditions: $J + J_1 = 5.9$ kg·m^2 and $\omega = \pi$ rad/s.

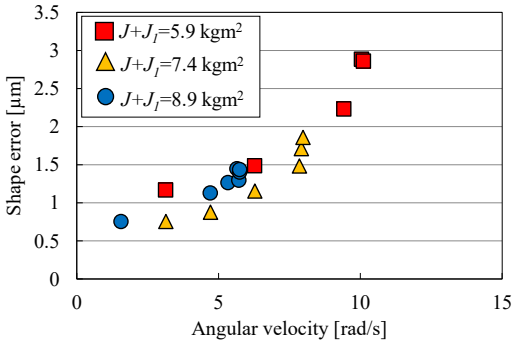

Fig. 14. Experimental results for the shape error under various conditions.

dynamic characteristics of the rotary axis and the linear axes. This error can easily be avoided by not contacting the part with the machining tool at a transient location on the axes; thus, in this study, we focused on a steady-state.

Figures 14 and **15** show the relationship between the average of the half-amplitude of the shape errors and the average of the relative angle differences, respectively, and the angular velocity under different moments of inertia. It

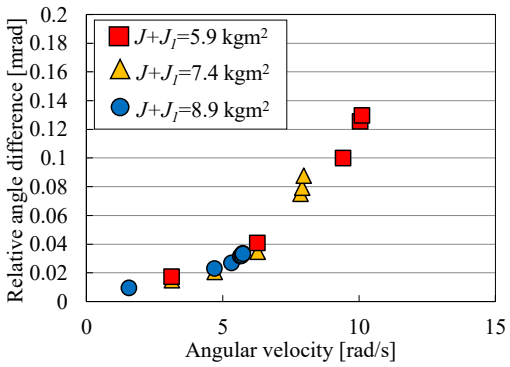

Fig. 15. Experimental results for the relative angle difference under various conditions.

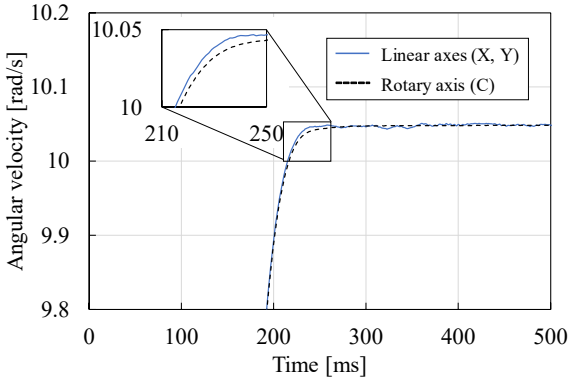

Fig. 16. Angular velocity on each axis under the following conditions: $J+J_1 = 5.9$ kg·m^2 and $\omega = 3.2\pi$ rad/s.

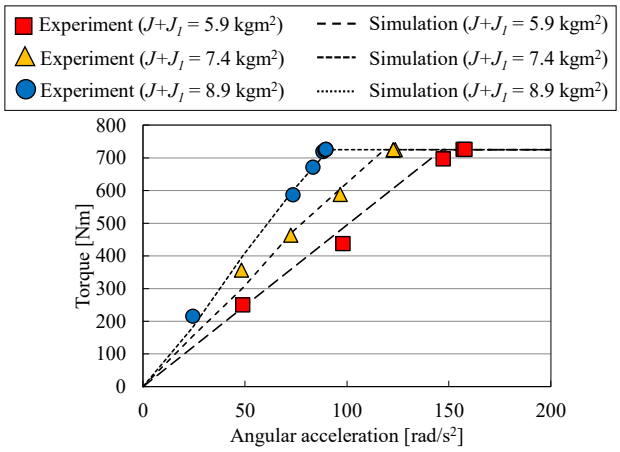

Fig. 17. Experimental and simulation results for the torque.

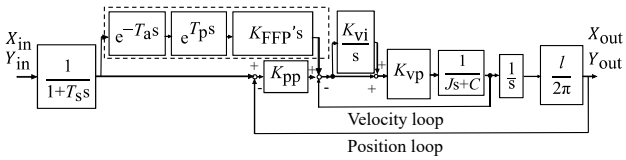

(a) Linear axes

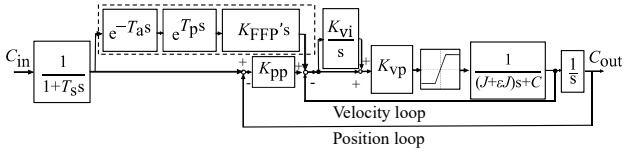

(b) Rotary axis

Fig. 18. Revised block diagrams of the feed drive system.

is important to consider the maximum and minimum values of the shape error; thus, high importance was placed on the average of the half-amplitude of the shape error. According to these results, a higher the angular velocity ω corresponded to larger average values of the relative angle difference $(\alpha-\beta)$ and a larger magnitude of the shape errors at the half-amplitude.

To ascertain the cause of the observed relative angle difference, the angular velocity of each axis was investigated under the following conditions: $J+J_1 = 5.9$ kg·m^2, $\omega = 3.2\pi$ rad/s, and $d\omega/dt = 3.2\pi/0.064$ rad/s^2. **Fig. 16** depicts the experimental results. The time at which the linear axes moved at the intended angular velocity was 236 ms, although the rotary axis needed 263 ms to move at the same angular velocity. Thus, it can be stated that the rotary axis followed the target angular velocity less effectively than the linear axes. This behavior indicates that the average values of the relative angle difference $(\alpha-\beta)$ became large.

5.2. Suggestion of Models Considering Torque Saturation

Next, the reason why the rotary axis poorly followed the target angular velocity at high values was examined. A phenomenon called torque saturation occurs when a torque order exceeds the limits of a servo system, reducing the ability of the axis to follow when under the precedent control [21]. In general, this tends to occur in DD motor systems. Therefore, the torque of the rotary axis was the focus of this part of the investigation.

The plots in **Fig. 17** depict the torque of the rotary axis at different angular velocities, as determined by an experiment. The angular acceleration $(d\omega/dt)$ was obtained by calculating the maximum value of the second-order derivative of the displacement of the rotary axis with respect to time. The dashed lines in **Fig. 17** represent the simulated results for the rotary axis torque based on the block diagram in **Fig. 18**. From **Fig. 17**, 725 Nm can be verified as the torque saturation value using the experimental results for the torque under the following conditions: $J+J_1 = 5.9$ kg·m^2 and $\omega = 3.2\pi$ rad/s (**Fig. 19**). Moreover, according to **Fig. 17**, the angular acceleration at which torque saturation occurs can be estimated. For example, torque saturation occurs at $d\omega/dt$ =146.7, 118.5, and 91.1 rad/s^2 when the moments of inertia are $J+J_1 = 5.9$, 7.4, and 8.9 kg·m^2, respectively.

The dashed lines in **Fig. 20** represent the simulated average values of the relative angle difference $(\alpha-\beta)$ calculated as shown in **Fig. 18**. The plots in **Fig. 20** present

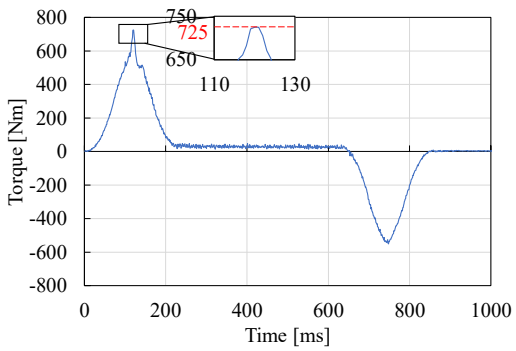

Fig. 19. Experimental results for the motor torque under the following conditions: $J+J_1 = 5.9$ kg·m^2 and $\omega = 3.2\pi$ rad/s.

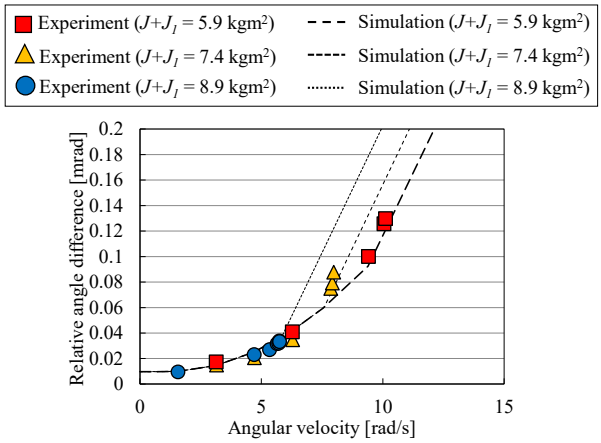

Fig. 20. Experimental and simulation results for the relative angle difference in various states.

the experimental results provided in **Fig. 15** for comparison. From **Fig. 20**, it is clear that the experimental and simulated results agreed well, and the average values of the relative angle difference ($\alpha - \beta$) were estimated by applying the block diagram in **Fig. 18**, which addresses the torque saturation of the rotary axis. The torque saturation occurred at $\omega = 9.39$, 7.58, and 5.83 rad/s when the moments of inertia were $J+J_1 = 5.9$, 7.4, and 8.9 kg·m^2, respectively. **Fig. 21** depicts the relationship between R_C and ω_R, as shown in **Fig. 5,** where torque saturation occurred. As indicated by **Fig. 21**, torque saturation occurred during machining at $R_C = 0.36$, 0.44, and 0.57 mm when the moments of inertia were $J+J_1 = 5.9$, 7.4, and 8.9 kg·m^2, respectively, at an end milling point feed speed of $F_C = 200$ mm/min.

5.3. Applying Best K_{FFP} Method

Next, using the proposed models, the potential reduction in the shape error was estimated using the Best K_{FFP} Method (Eq. (20)). **Fig. 22** shows the optimal K_{FFP} values calculated using the Best K_{FFP} Method. **Fig. 23** depicts the relative angle difference (vertical axis) over time (horizontal axis) before and after an optimal K_{FFP} was applied, under the following conditions: $J+J_1 = 5.9$ kg·m^2,

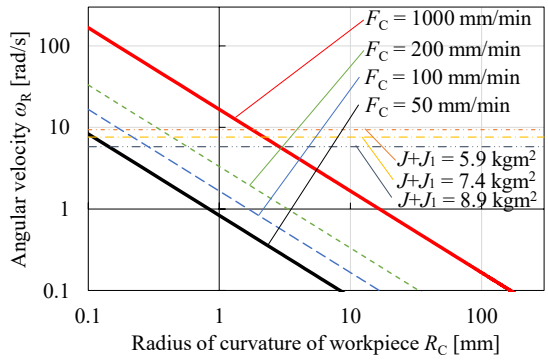

Fig. 21. Relationship between R_C and ω_R in consideration of the inflection point.

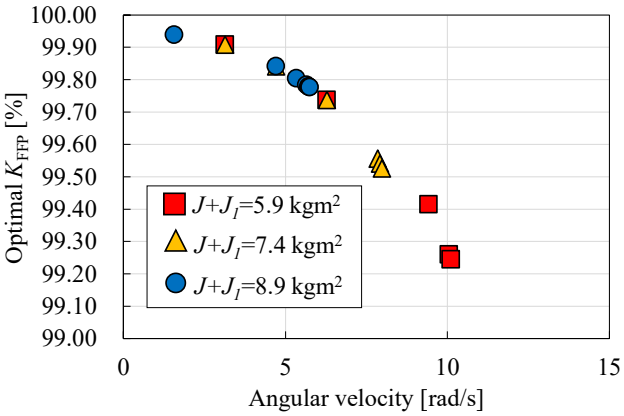

Fig. 22. Optimal values of K_{FFP}.

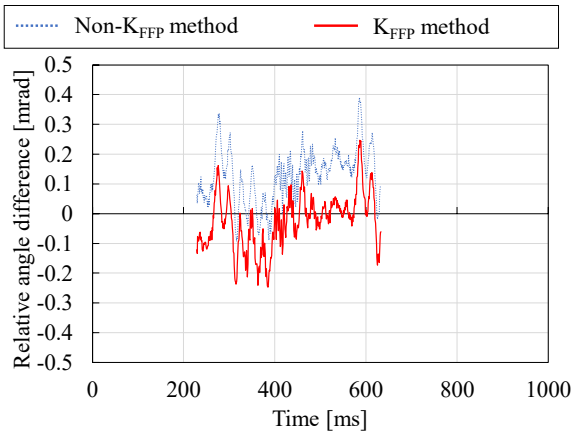

Fig. 23. Relative angle difference in setting the optimal K_{FFP} under the following conditions: $J+J_1 = 5.9$ kg·m^2 and $\omega = 3.2\pi$ rad/s.

$\omega = \pi$ rad/s, and $d\omega/dt = \pi/0.064$ rad/s^2. **Fig. 24** depicts the angular velocity (vertical axis) of the rotary and linear axes over time (horizontal axis) under the same conditions. **Fig. 25** depicts the shape error (vertical axis) over time (horizontal axis) before and after the optimal K_{FFP} was applied. Clearly, by applying an optimal K_{FFP} that was lower than the default value of 100%, the time at which the linear axes moved at the intended angular ve-

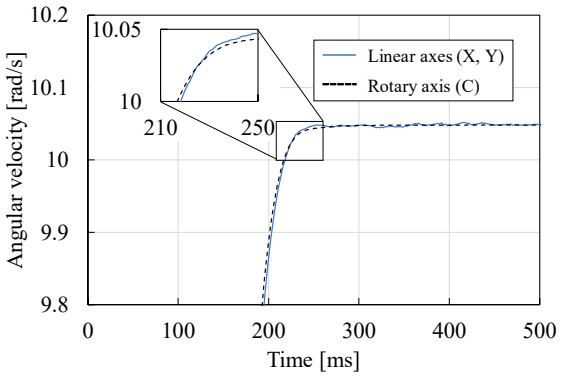

Fig. 24. Angular velocity on each axis in setting the optimal K_{FFP} under the following conditions: $J+J_1 = 5.9$ kg·m^2 and $\omega = 3.2\pi$ rad/s.

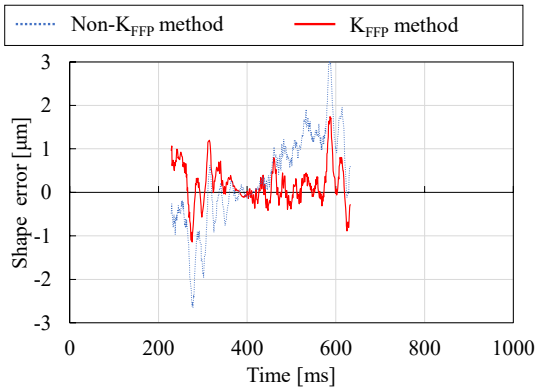

Fig. 25. Shape error in setting the optimal K_{FFP} under the following conditions: $J+J_1 = 5.9$ kg·m^2 and $\omega = 3.2\pi$ rad/s.

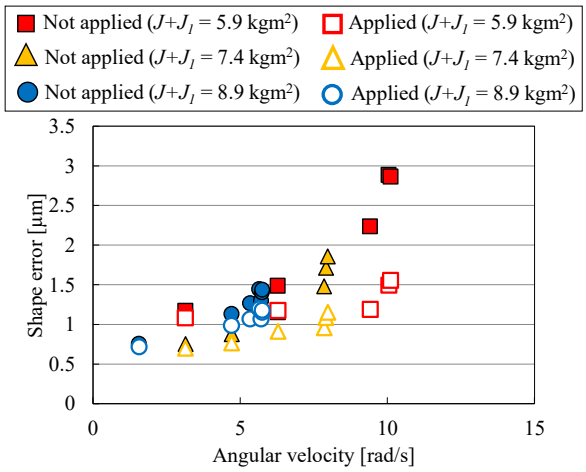

Fig. 26. Experimental results for the shape error under the optimal K_{FFP} method in various states.

locity was delayed, as shown in **Fig. 24**. As indicated by **Fig. 23**, the relative angle difference was reduced owing to this delay. Consequently, the shape error was reduced, as shown in **Fig. 25**. **Fig. 26** shows the shape errors obtained using the optimal K_{FFP} values for various conditions. The results were obtained as the average results of five repeated calculations for verification of the reproducibility. According to these results, the shape errors were improved for all conditions by applying the Best K_{FFP} Method. This successful improvement under conditions of a high-angular-velocity was realized by using the block diagram shown in **Fig. 18**, as it addresses torque saturation.

6. Conclusions

A 5MC equipped with a precedent control (Pre-Control) function was evaluated during a CNC process, and the results were analyzed to improve the machined shape error. Under a constant feed speed vector at the cutting point, the factors contributing to the shape error were a decrease in radius and a relative angle difference between the rotary and linear axes. To reduce the influence of these factors even under high-angular-velocity conditions, the optimal K_{FFP} (precedent control coefficient) of each axis was determined via calculations using a derived block diagram considering the torque saturation in a DD motor rotary axis based on modeling of the precedent control. This method resulted in improved machining accuracy in the 5MC CNC process without sacrificing speed or efficiency.

References:

[1] Y. Ihara, K. Tsuji, and T. Tajima, "Ball bar measurement of motion accuracy in simulating cone frustum cutting on multi-axis machine tools," Int. J. Automation Technol., Vol.11, No.2, pp. 197-205, 2017.

[2] T. Nishiguchi, S. Hasegawa, R. Sato, and K. Shirase, "Evaluation method for behavior of rotary axis around motion direction changing," Int. J. Automation Technol., Vol.11, No.2, pp. 171-178, 2017.

[3] E.-Y. Heo, D.-W. Kim, B.-H. Kim, D.-K. Jang, and F. Frank, "Efficient rough-cut plan for machining an impeller with a 5-axis NC machine," Int. J. of Computer Integrated Manufacturing, Vol.21, No.8, pp. 971-983, 2008.

[4] N. Natsume, K. Nakamoto, T. Ishida, and Y. Takauchi, "Tool path generation for five-axis control semi finishing by use of square end mill," Trans. of the Japan Society of Mechanical Engineers, Series C, Vol.78, No.793, pp. 3305-3316, 2012 (in Japanese).

[5] J. T. Alves, M. Guingand, and J.-P. de Vaujany, "Designing and manufacturing spiral bevel gears using 5-axis computer numerical control (CNC) milling machines," J. of Mechanical Design (ASME), Vol.135, No.2, 024520, 2013.

[6] J. Chaves-Jacob, G. Poulachon, and E. Duc, "Optimal strategy for finishing impeller blades using 5-axis machining," The Int. J. of Advanced Manufacturing Technology, Vol.58, Nos.5-8, pp. 573-583, 2012.

[7] R. J. Bickel and M. Tomizuka, "Synchronization of multiple-axis system subject to periodic disturbances," ASME Japan/USA Symp. Flexible Automation, Vol.2, p. 821, 1992.

[8] A. Matsubara, "Design and Control of Precision Positioning and Feed Drive System," p. 78, 214-218, Morikita Publishing, 2008 (in Japanese).

[9] T. Hirogaki, E. Aoyama, K. Ogawa, T. Kawaguchi, and T. Horiuchi, "Investigation on end-mill cutter location based on constant feed-speed vector at cutting point with a five-axis machining center," J. of the Japan Society for Precision Engineering, Vol.76, No.8, pp. 912-917, 2010 (in Japanese).

[10] T. Kaneeda and Y. Oe, "Lubricant applying effect in ductile metal cutting (3rd report) – Investigation of role of lubricant applying effect in lubrication by oil-submerged cutting –," J. of the Japan Society for Precision Engineering, Vol.68, No.4, pp. 566-570, 2002 (in Japanese).

[11] T. Hirogaki, Y. Nakamura, T. Horiuchi, E. Aoyama, and K. Ogawa, "Optimization of acceleration and deceleration processing suited to simultaneous control with five-axis machining center," Proc. of 15th Int. Conf. on Advances in Materials & Processing Technologies (AMPT 2012), 26768, Wollongong, Australia, September 2012.
[12] T. Hirogaki, "Effect of simultaneous control in constant direction of feed at cutting point to machined two-dimensional line-shapes," Proc. of 2010 ISFA, JPL-2496, pp. 1-7, 2010.
[13] J. Vinvancos, C. J. Luis, J. A. Ortiz, and H. A. González, "Analysis of factors affecting the high-speed side milling of hardened die steels," J. of Materials Processing Technology, Vols.162-163, No.15, pp. 696-701, 2005.
[14] R. Sato, Y. Yokobori, and M. Tsutsumi, "Dynamic synchronous accuracy of translational axes and rotational axes in 5-axis machining center," J. of the Japan Society for Precision Engineering, Vol.72, No.1, pp. 73-78, 2006 (in Japanese).
[15] R. V. Fleisig and A. D. Spence, "A constant feed and reduced angular acceleration interpolation algorithm for multi-axis machining," Computer-Aided Design, Vol.33, No.1, pp. 1-15, 2001.
[16] T. Yamazaki, M. Seto, and M. Tsutsumi, "Design of acceleration and deceleration commands for NC machine tools," J. of the Japan Society for Precision Engineering, Vol.66, No.8, pp. 1260-1264, 2000 (in Japanese).
[17] Y. Kakino, T. Ihara, and Y. Nakatsu, "A study on the motion accuracy of NC machine tools (2nd report) – Diagnosis of motion error origins by using double ball bar test –," J. of the Japan Society for Precision Engineering, Vol.52, No.10, pp. 1739-1745, 1986 (in Japanese).
[18] T. Suzuki, Y. Maruyama, T. Hirogaki, and E. Aoyama, "Improvement of machining accuracy under constant feed speed at milling point with a five-axis controlled machining center based on advanced control method," Trans. of the Japan Society of Mechanical Engineers, Series C, Vol.83, No.849, pp. 1-15, 2017 (in Japanese).
[19] K. Erkorkmaz and Y. Altintas, "High speed CNC system design part II: modeling and identification of feed drives," Int. J. of Machine Tools and Manufacture, Vol.41, No.10, pp. 1487-1509, 2001.
[20] J.-S. Chen, Y. K. Hung, and C.-C. Cheng, "Mechanical model and contouring analysis of high-speed ball-screw drive system with compliance effect," The Int. J. of Advanced Manufacturing Technology, Vol.24, Nos.3-4, pp. 241-250, 2004.
[21] D. Endo, R. Sato, and M. Tsutsumi, "High performance motion control of rotary axis for simultaneous multi-axis motion," J. of the Japan Society for Precision Engineering Spring Conf., pp. 135-136, 2007 (in Japanese).

Name:
Takamaru Suzuki

Affiliation:
Ph.D. Student, Doshisha University

Address:
1-3 Tataramiyakodani, Kyotanabe-shi, Kyoto 610-0394, Japan

Brief Biographical History:
2018- Ph.D Student, Doshisha University

Main Works:
• "Improvement of machining accuracy under constant feed speed at milling point with a five-axis controlled machining center based on Advanced control Method," Trans. of the Japan Society of Mechanical Engineers, Series C, Vol.83, No.849, pp. 1-15, 2017.

Membership in Academic Societies:
• Japan Society of Mechanical Engineers (JSME)
• Japan Society for Precision Engineering (JSPE)

Name:
Kazuki Yoshikawa

Affiliation:
Master Course Student, Doshisha University

Address:
1-3 Tataramiyakodani, Kyotanabe-shi, Kyoto 610-0394, Japan

Brief Biographical History:
2016- Master Course Student, Doshisha University

Main Works:
• "Estimation of machined accuracy under constant feed speed vector at milling point with a five-axis controlled machining center," 17th Int. Conf. on Precision Engineering (ICPE2018), Kamakura, Japan, November 2018.

Membership in Academic Societies:
• Japan Society of Mechanical Engineers (JSME)
• Japan Society for Precision Engineering (JSPE)

Name:
Toshiki Hirogaki

Affiliation:
Professor, Faculty of Science and Engineering, Doshisha University

Address:
1-3 Tataramiyakodani, Kyotanabe-shi, Kyoto 610-0394, Japan

Brief Biographical History:
1990- Mitsubishi Motors Corporation
1993- Technology Research Institute of Osaka Prefecture
1995- The University of Shiga Prefecture
2006-2007 Visiting Researcher, University of California, Berkeley
2003- Doshisha University

Main Works:
• "Environmental Impact of Desktop-Sized Five-Axis CNC Machine Tool Estimated with LCA," J. of Environment and Engineering, Vol.6, No.2, pp. 242-252, 2011.
• "Control of Percussion Motion by Sound Feedback with a Humanoid Robot," J. of Key Engineering Materials (Emerging Technology in Precision Engineering XIV), Vols.523-524, pp. 699-704, 2012.
• "Investigation of Temperature Hysteresis on Tooth Contact Surface of Hypoid Gears using Middle-Infrared Ray Imagery Based on Thermal Network model," J. of Advanced Mechanical Design, Systems, and Manufacturing, Vol.8, No.3, pp. 1-15, 2014.
• "Investigation of Step Micro-Drilling Motion Based on Modeling of High Speed Spindle Driving Axis on Machine Tools Equipped with Vibration-Proof Mechanism," J. of Advanced Materials Research, Vol.1017, pp. 642-647, 2014.
• "Influence of Ball Screw Equipped with Counter-Balance Mechanism on Machine Tool Vibration in Step-Drilling Process," J. of Manufacturing Science and Technology, Vol.3, No.5, doi: 10.13189/mst.2015.030512, pp. 266-273, 2015.
• "Investigation of Control Methods of Chatter Vibration Based on Analysis of End-Milling Chatter Mark," J. of Advanced Materials Research, Vol.1136, pp. 639-644, 2016.
• "Monitoring of Rotational Vibration in Tap and Endmill Processes with a Wireless Multifunctional Tool Holder System," Int. J. Automation Technol., Vol.12, No.6, pp. 876-882, 2018.

Membership in Academic Societies:
• Japan Society of Mechanical Engineers (JSME)
• Japan Society for Precision Engineering (JSPE)
• Society of Materials Science, Japan (JSMS)
• Japan Institute of Electronics Packaging (JIEP)

Name:
Eiichi Aoyama

Affiliation:
Professor, Faculty of Science and Engineering, Doshisha University

Address:
1-3 Tataramiyakodani, Kyotanabe-shi, Kyoto 610-0394, Japan

Brief Biographical History:
1977- Technology Research Institute of Osaka Prefecture
1997- 1998 Visiting Researcher, Queen Mary & Westfield College, University of London
1987- Doshisha University

Main Works:
• "Development of nanofiber abrasive buffing pad produced with modified melt blowing method," Int. J. of Abrasive Technology, Vol.9, No.1, pp. 31-48, 2019.
• "Development of Polishing Tool Capable of Self-Adaptive to Processing Site Using Steel Balls and Magnetic Force," J. of Advanced Materials Research, Vol.1136, pp. 466-471, 2016.
• "Estimation of Micro-Hole Shape in Laser Direct Drilling of High Heat Radiation Typed Printed Circuit Boards (Process Monitoring with a High Speed Camera)," J. of Key Engineering Materials (Precision Engineering and Nanotechnology V), Vol.625 , pp. 172-177, 2014.
• "An Indicative End-Milling Condition Decision Support System Using Data-Mining for Difficult-to-Cut Materials Based on Comparison with Irregular Pitch and Lead End-Mill and General Purpose End-Mill," J. of Advanced Materials Research, Vol.797, pp. 177-182, 2013.
• "Surface Generation for Magic-Mirror by End-Milling and Magnetic Polishing with Digitally Functioned CNC Machining Center," J. of Key Engineering Materials (Emerging Technology in Precision Engineering XIV), Vols.523-524, pp. 368-373, 2012.

Membership in Academic Societies:
• Japan Society of Mechanical Engineers (JSME)
• Japan Society for Precision Engineering (JSPE)
• Japan Society for Abrasive Technology (JSAT)
• Society of Materials Science, Japan (JSMS)

Name:
Takakazu Ikegami

Affiliation:
Doctor of Engineering, DMG MORI Co., Ltd.

Address:
362 Idono-cho, Yamatokoriyama, Nara 639-1183, Japan

Brief Biographical History:
2005- DMG MORI Co., Ltd.
2014- Ph.D. Student, Doshisha University

Main Works:
• "Development of direct drive motor for machine tools and consideration of its performance in machining," J. of the Japan Society for Abrasive Technology, Vol.60, No.6, pp. 333-337, 2016.

Membership in Academic Societies:
• Japan Society of Mechanical Engineers (JSME)
• Japan Society for Precision Engineering (JSPE)
• Japan Society for Abrasive Technology (JSAT)